Colloids and Surfaces B: Biointerfaces 205 (2021) 111835

Contents lists available at ScienceDirect

Colloids and Surfaces B: Biointerfaces

journal homepage: www.elsevier.com/locate/colsurfb

A colorimetric alkaline phosphatase biosensor based on *p*-aminophenol-mediated growth of silver nanoparticles

Samy M. Shaban [a,b,c,1], Byeong-Seok Moon [a,1], Do-Gi Pyun [d], Dong-Hwan Kim [a,b,*]

[a] School of Chemical Engineering, Sungkyunkwan University, 16419, Republic of Korea
[b] Biomedical Institute for Convergence at SKKU (BICS), Sungkyunkwan University, 16419, Republic of Korea
[c] Petrochemical Department, Egyptian Petroleum Research Institute, Egypt
[d] Biomedical Polymer R&D institute, T&L Co., Ltd, Anseong, 17554, South Korea

ARTICLE INFO

Keywords:
Silver nanoparticles
Alkaline phosphatase
Colorimetric sensor
p-aminophenol
Localized surface plasmon resonance

ABSTRACT

Alkaline phosphatase (ALP) is an enzyme that catalyzes the dephosphorylation of proteins, nucleic acids, and biomolecules. It is a potential biomarker for diverse diseases such as breast cancer, osteopenia, and hepatobiliary. Herein, we developed a colorimetric sensor for the ALP assay based on its enzymatic activity to dephosphorylate the *p*-aminophenol phosphate (*p*APP) into *p*AP. In a solution containing silver nanoparticles (AgNPs) and Ag^+ ions prepared using a low concentration of $NaBH_4$, *p*AP mediates the growth of AgNPs by reducing the concentration of Ag^+ ions to enhance the intensity of localized surface plasmon resonance as the *p*APP cannot induce a reduction of the remaining Ag^+ due to the masking of the hydroxyl with phosphate. The quantitative assay of the ALP was demonstrated via the colorimetric detection of the *p*AP-mediated growth of AgNPs in the presence of an ALP. The highly sensitive enzymatic growth of AgNPs provided a wider dynamic linear range of 0.5–225 U/L with a lower limit of detection of 0.24 U/L than that previously reported. The use of *p*AP resulted in excellent selectivity of the sensor for the ALP assay in human serum, yielding a high recovery rate and a high precision of 99.2 ± 1.5 % for the standard addition method.

1. Introduction

Alkaline phosphatase (ALP) is an enzyme that can eliminate phosphate groups in proteins, nucleic acids, and biomolecules, which is crucial to sustain the metabolism of living organisms. Therefore, ALP is detected in the intestine, liver, kidney, bone, and placental tissues in the human body [1–4]. ALP is considered to be an important prognostic (and diagnostic) biomarker because the abnormal expression of ALP indicates the presence of certain diseases like breast and prostatic cancer, bone disease, and hepatobiliary disease [5–10]. The normal level of ALP in adult human serum is 40–190 U/L (and is more than 500 U/L for children and pregnant women) [11]. A higher level of ALP typically indicates the presence of osteoblastic bone tumors [12,13], biliary obstruction [14,15], and diabetes [16,17], whereas a lower level is associated with some metabolic disorders or Wilson's disease [7,18]. ALP has recently been presented as a label enzyme to replace horseradish peroxidase (HRP) enzymes in immunoassay systems (ELISA) [19–22]. HRP enzymes have been extensively used in ELISA because of their small size, high turnover value, high stability, and low stearic hindrance. However, it has been reported that HRP interferes with antibacterial agents containing azides, cyanides, and sulfides. HRP also releases mutagenic and carcinogenic products upon reacting with the HRP substrate [23,24]. These drawbacks of HRP have prompted the usage of the ALP enzyme as an alternative to the HRP enzyme in immunoassay systems. Therefore, there have been considerable efforts to develop biosensors for the ALP assay via various detection strategies, such as fluorometry [25–28], Raman scattering [29–31], capillary electrophoresis [32–34], and electrochemical reactions [35–37]. Compared with other techniques, colorimetric ALP biosensors, which exploit the chromogenic signals between the phosphate substrate and the dephosphorylated products, enable much simpler and faster quantitative detection of ALP with less complex instrumentation, making them suitable for point-of-care testing systems.

A variety of phosphate molecules, such as *p*-nitrophenyl phosphate, disodium phenyl phosphate, and ascorbic acid phosphate, have been explored as a substrate for ALP biosensors [38–40]. Among these,

* Corresponding author at: School of Chemical Engineering, Sungkyunkwan University, 16419, Republic of Korea.
E-mail address: dhkim1@skku.edu (D.-H. Kim).
[1] These authors have contributed equally to this work.

https://doi.org/10.1016/j.colsurfb.2021.111835
Received 19 December 2020; Received in revised form 14 April 2021; Accepted 8 May 2021
Available online 11 May 2021

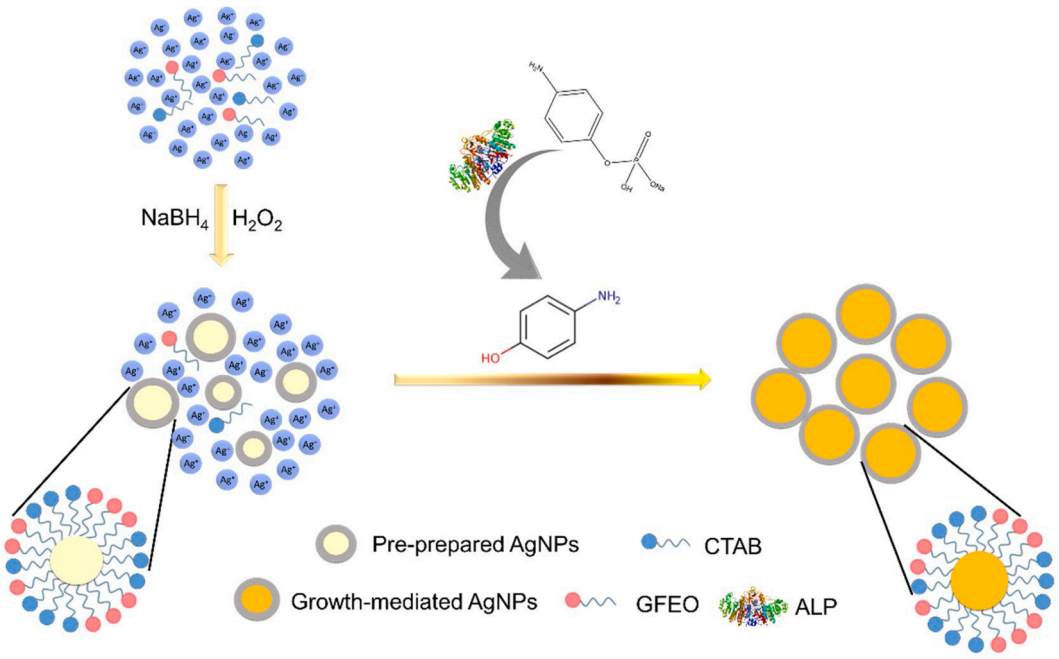

Scheme 1. Schematic representation of ALP detection based on the *p*AP-mediated growth of AgNPs.

ascorbic acid phosphate, which is hydrolyzed into ascorbic acid by ALP, is the most commonly used substrate because it provides high reducing power for transducing chemical signals to optical or electrical signals [41–47]. However, the level of ascorbic acid is highly dependent on the nutrition condition of patients, leading to false-positive results in the ALP assay [48–51]. Therefore, an alternative phosphate substrate is required to develop highly sensitive and reproducible ALP biosensors.

Herein, we developed a colorimetric biosensor for the ALP assay based on its enzymatic activity to convert *p*-aminophenol phosphate (*p*APP) into *p*AP. *p*AP can mediate the controlled growth of AgNPs from a solution containing an AgNPs–Ag^+ mixture that is prepared using a low concentration of $NaBH_4$. The *p*AP-mediated growth of AgNPs enhances the intensity of localized surface plasmon resonance (LSPR) with a distinct color change as a function of *p*AP concentration. The developed colorimetric ALP biosensor used herein is highly sensitive with a low limit of detection (LOD) of 0.24 U/L with an UV–vis spectrometer and 30 U/L with a naked-eye readout. We also found that *p*AP is highly selective to the ALP detection, resulted in a reproducible ALP assay in diluted human serum (10 %) with a high recovery rate of 99.2 ± 1.5 % for the standard addition method.

2. Materials and methods

2.1. Materials

Silver nitrate ($AgNO_3$), magnesium chloride anhydrous ($MgCl_2$), *p*-aminophenol (*p*AP), cetyl trimethyl ammonium bromide (CTAB), p-aminophenyl phosphate monosodium (*p*APP), sodium boron hydride ($NaBH_4$), alkaline phosphatase (ALP), penicillin-streptomycin (penicillin), thrombin (Thr), bovine serum albumin (BSA), glucose oxidase (GOX), matrix metallopeptidase 9 (MMP-9), and human immunoglobulin G (IgG) were purchased from Sigma Aldrich, whereas trypsin (Try) was purchased from ThermoFisher. All solvents and chemicals were used as received without purification. Deionized water filtered to 18.2 MΩ.cm was used in all experiments.

2.2. Preparation of gemini nonionic (GFEO) surfactant

The gemini nonionic (GFEO) surfactant was synthesized in the laboratory using a procedure described in [52]. Fumaric acid was esterified with 3-(4-hydroxyphenyl) propanoic acid in the presence of p-toluenesulfonic acid as a catalyst, and xylene was used as a solvent. The theoretical volume of water was collected in the Dean–Stark apparatus to obtain the diester and the intermediate compound. After evaporating the solvent and performing recrystallization using diethyl ether, the intermediate compound was esterified with polyethylene glycol using the same conditions as in the fumaric acid esterification. After the reaction, the obtained product was treated like the aforementioned intermediate compound and the product was dissolved in xylene with dodecanoic acid and *p*-toluenesulfonic acid as a catalyst. Diethyl ether was used for recrystallization after evaporating the solvent and performing purification. The resulting compound was labeled as GFEO surfactant.

2.3. Preparation of the AgNPs–Ag^+ solution

An aqueous solution of $AgNO_3$ precursor (50 mL, 0.9 mM) was mixed with 3 mL of an aqueous GFEO surfactant solution (1 mM) and 1 mL of aqueous CTAB solution (10 mM). Then, the solution was stirred for 8 min at 1100 rpm. Subsequently, 120 μL of hydrogen peroxide (35 %) was added to the aforementioned solution with stirring, followed by the addition of 330 μL of $NaBH_4$ (0.1 mM). The color of the solution instantly changed from colorless to faint yellow.

2.4. Characterization of AgNPs

The morphology of the prepared AgNPs was imaged using a transmission electron microscope (TEM, JEM-ARM200 F, JEOL). The Zetasizer (Malvern) was used to examine the size distribution of the synthesized nanoparticles and their zetapotential. The LSPR of the nanoparticles was monitored using a UV–vis spectrometer (V770, JASCO).

2.5. ALP assay based on the pAP-mediated growth of AgNPs

Fixed volumes (50 μL) of ALP at different concentrations (0–450 U/L) in Tris-base solution (10 mM, pH = 9.5) were mixed with 50 μL of *p*APP aqueous solution (3 mM), and this solution was incubated for 30

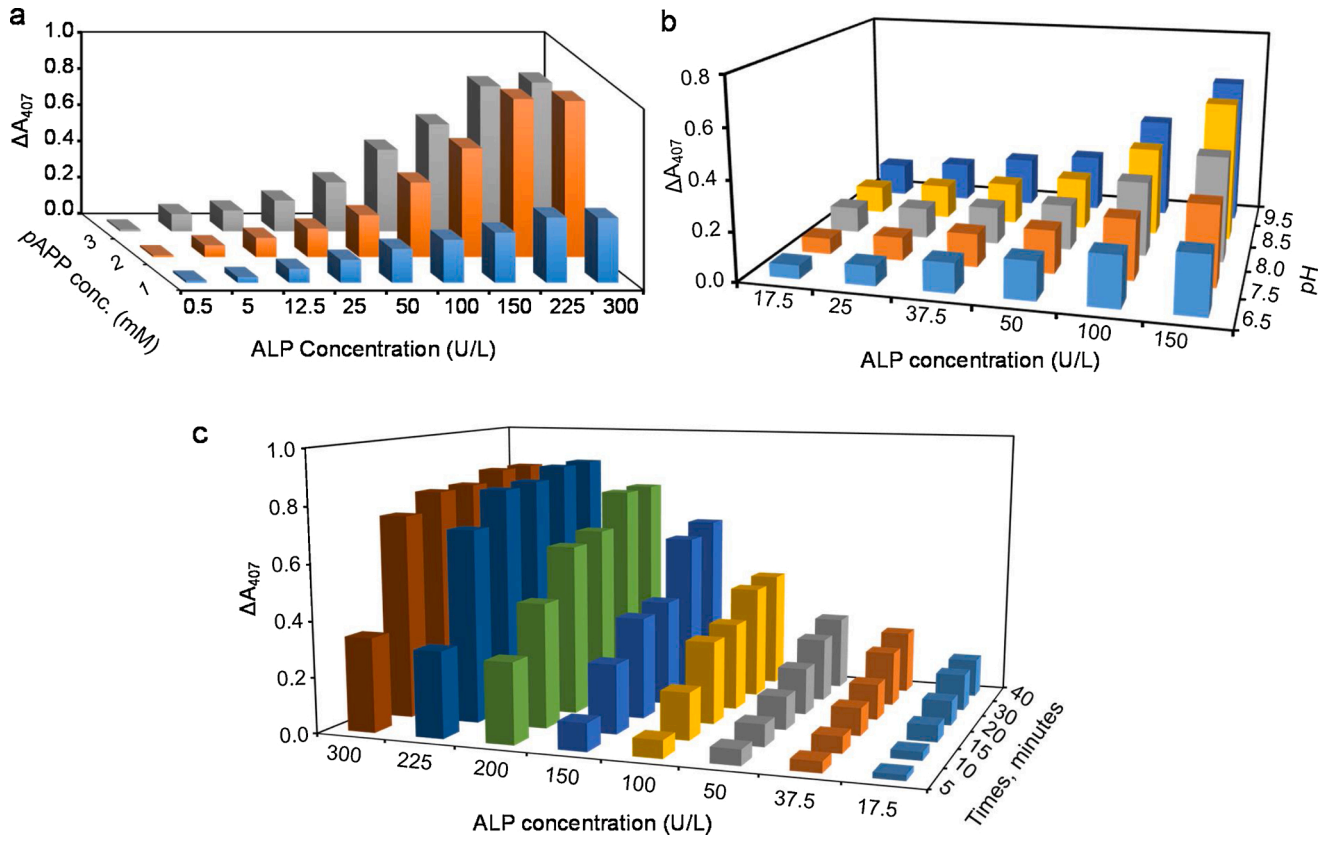

Fig. 1. Optimization of the ALP assay conditions. Effect of the **(a)** initial *p*APP substrate concentration (**b**) pH of the medium and (**c**) incubation time were investigated.

min at 37 °C in a water bath. After the incubation period, 1 mL of the as-prepared AgNPs–Ag^+ solution was injected into the aforementioned solution. The change in color and absorbance of the solution was measured using the naked eye and UV–vis spectroscopy, respectively, after 5 min for the *p*AP-mediated growth of AgNPs.

2.6. Selectivity for ALP assay

Seven different biomolecular species, namely, penicillin, Try, Thr, BSA, MMP-9, GOX, and IgG, which are commonly present in human serum, were selected to investigate their interference with the developed ALP biosensor. They were individually tested as an alternative to ALP under the same conditions as mentioned in Section 2.5. Subsequently, the ALP assay was conducted with the species, and the results were compared with the case wherein there were no species present.

2.7. ALP assay in human serum

Human serum was used without any pretreatment. It was diluted 10 times using the Tris-base solution (10 mM, pH = 9.5) prior to conducting the ALP assay using the same procedure as mentioned in Section 2.5, except that 50 μL of the standard ALP was replaced with 50 μL of the diluted human serum. A standard solution of ALP was added to the reaction solution to evaluate the recovery rate. The recovery rate (%) was calculated according to the following equation:

$$\text{Recovery rate } (\%) = \frac{\text{Measured concentration}}{\text{Added concentration}} \times 100$$

3. Results and discussion

3.1. pAP-mediated growth of AgNPs

A solution containing an AgNPs–Ag^+ mixture was prepared using small concentrations of $NaBH_4$, which is insufficient for the consumption of all Ag^+ ions. The addition of hydrogen peroxide allowed for the further growth of AgNPs via the reduction of the remaining Ag^+ ions [45]. The prepared AgNPs–Ag^+ solution was kept in a refrigerator before use, and it showed no change in both its color and peak intensity at λ =407 nm for two months. This solution can be used as a colorimetric indicator of ALP when it is injected into the mixture of *p*APP and ALP because *p*AP, which is released from *p*APP by the action of ALP, reduces Ag^+ ions for the further growth of AgNPs, resulting in the LSPR enhancement of AgNPs for the colorimetric detection of ALP (Scheme 1).

In our ALP sensing scheme, the uniformity of the AgNP seeds in the prepared solution should be precisely controlled to maximize sensitivity to *p*AP because the growth of AgNPs depends on the size and shape of the AgNP seeds. To attain the uniformity in AgNP seeds, we employed a binary surfactant system (comprising CTAB and GFEO surfactants), which allows for better control of kinetics in nanoparticle formation and growth for fine tuning [53–55]. Compared with the irregular morphology and large size of AgNPs of the single surfactant systems (Figure S1 and S2 for the CTAB and GFEO surfactants, respectively), the simultaneous use of the CTAB and GFEO surfactants resulted in AgNPs of a small size exhibiting a uniform spherical nanostructure, as depicted in Figures S3a and S4a. The small size of the AgNPs is attributed to the use of the two different surfactants, leading to decreased solution interfacial tension and enhanced adsorption tendency of the surfactant toward interfaces. Thus, in the case of using a mixed surfactant, their adsorption affinity toward the initially formed AgNP surface is increased, thereby suppressing AgNPs agglomeration and preventing the formation of

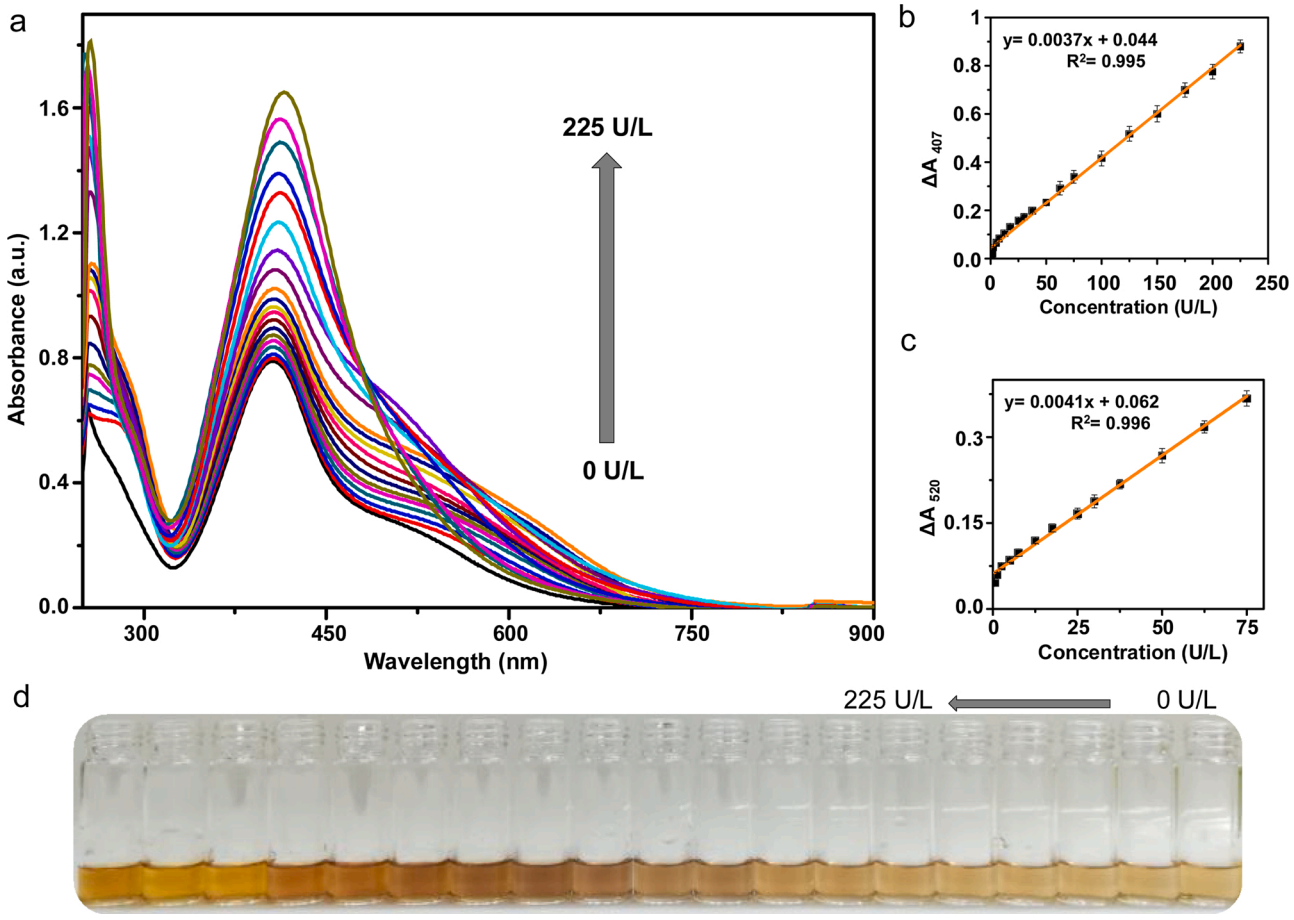

Fig. 2. (**a**) UV–vis spectra of the colorimetric ALP biosensor based on the *p*AP-mediated growth of AgNPs, with different concentrations of ALP and corresponding calibration curve showing the change in the absorbance of the biosensor at a wavelength of **(b)** 407, and (**c**) 520 nm as a function of ALP concentration. (**d**) Photograph of the color change of the sensor with different concentrations of ALP. The concentrations of ALP are 0, 0.5, 1.25, 2.5, 5, 7.5, 12.5, 17.5, 25, 30, 37.5, 50, 62.5, 75, 100, 125, 150, 175, 200, and 225 U/L.

bigger AgNPs [53,56,57]. After the reaction of the uniform AgNP seeds-Ag^+ ions and *p*AP (85 μM), we confirmed the *p*AP-mediated growth of AgNPs via TEM imaging and particle-size estimation (with an increase in the average size of AgNPs) as depicted in Figures S3b and S4b, clarifying that our strategy works successfully.

3.2. Colorimetric ALP biosensor based on the pAP-mediated growth of AgNPs

Scheme 1 describes the principle of the ALP assay through an enzymatic reaction. The ALP enzyme can catalyze the dephosphorylation of *p*APP substrate into the *p*AP, which has the ability to mediate an enhancing AgNPs growth of the prepared AgNPs–Ag^+ solution (Scheme 1). As the ALP concentration increases, the amount of the released *p*AP from *p*APP increases, followed by the increase in the LSPR peak intensity as a result of AgNP growth. *p*APP cannot mediate the growth of AgNPs because the phosphate group of *p*APP masks the hydroxyl group of *p*AP, thus preventing the release of the electron that is responsible for the reduction of Ag^+ into AgNPs. Based on that, the mediated-growth of AgNPs–Ag^+ by *p*AP can be used for ALP assay.

The enzymatic activity of ALP depends on several parameters that must be optimized for a successful ALP assay, such as incubation time between the ALP and phosphate substrate (*p*APP), pH of the environment, and concentration of initial *p*APP substrate. We optimized these factors to elucidate the best operation condition for the ALP assay, as shown in Fig. 1. As the *p*APP is considered as the source of reducing agent *p*AP, its concentration plays an important role in enhancing the sensor sensitivity. Upon increasing the concentration of *p*APP substrate to 3 mM, a continuous enhancement in the LSPR peak intensity at 407 nm occurred (Fig. 1a). When the *p*APP concentration was >3 mM, a background signal was observed even in the absence of ALP; thus, the optimal concentration of the *p*APP substrate is 3 mM. Fig. 1b shows the effect of pH on the catalytic performance of ALP toward converting the *p*APP into *p*AP. Upon increasing the environmental pH, the ALP activity enhanced, promoting a higher concentration of the released *p*AP. Thus, maximum change in the LSPR intensity of AgNPs occurred; as such, the pH of 9.5 was considered as optimal pH for highest ALP activity. As the reaction between the ALP and *p*APP is kinetically controlled, optimizing the incubation time is significant. Thus, under the optimized pH and pAPP concentration, the incubation time between ALP and *p*APP was investigated (Fig. 1c). Incubation time of 30 and 40 min induce similar changes in the LSPR intensity of AgNPs, indicating that both can lead to the same amount of *p*AP released; thus, 30 min was considered as the optimum incubation time between the *p*APP and ALP. Results determined the optimized condition for the ALP assay, as described in Section 2.5, i.e., incubation of 50 μL of ALP in Tris-base solution (pH = 9.5) for 30 min with 50 μL of *p*APP (3 mM) at 37 °C, followed by the addition of 1 mL of the prepared AgNPs–Ag^+ solution. Then, a change in the LSPR intensity at 407 nm and the color was detected through UV–vis spectrometry and the naked eye after a subsequent 5-min incubation.

Colorimetric detection of ALP based on the pAP-mediated growth of AgNPs was conducted, as shown in Fig. 2a. By increasing the concentration of ALP from 0.5–225 U/L, a significant change in the absorption intensity, which originates from the LSPR effect, with a slight red shift,

Table 1
Performance comparison of ALP biosensors.

Method	Linear range (U/L)	LOD (U/L)	Ref.
Colorimetric	0.5–225	0.24	This work
Colorimetric	0–120	5.4	[58]
Colorimetric	0–200	1.25	[59]
Colorimetric	5–100	3.3	[60]
Colorimetric	0.01–0.4	0.01	[44]
Colorimetric	0.2–20	0.1	[61]
Fluorescence	3.4–100	0.9	[62]
Fluorescence	17.6–782.6	1.1	[63]
Fluorescence	4.6–383.3	1.4	[64]
Fluorescence	0–150	0.15	[65]
Fluorescence	0−100	0.63	[66]
Fluorescence	0.2−100	0.06	[67]

was observed, indicating further growth of the prepared AgNPs. The change in the absorption intensity at 407 and 520 nm was measured for the quantitative detection of ALP, which is shown in Fig. 2b,c, with a linear dynamic range of 0.5–225 U/L (y = 0.0037x + 0.044) and 0.5–75 U/L (y = 0.0041x + 0.062) for 407 and 520 nm, respectively. The LOD was as low as 0.24 U/L based on the equation $3\sigma/m$ (σ is the standard deviation of the blank sample, and m is the slope of the calibration curve). The colorimetric response of the prepared AgNPs to ALP from yellow to brown is shown in Fig. 2d, which is useful for the colorimetric detection of ALP with naked eyes at an LOD of 30 U/L, where a yellow-to-brown color change was observed. The LOD of our ALP biosensor is lower than most of the previously reported ALP colorimetric sensors, including some of the fluorometric ones (Table 1), making it suitable for use as an ALP assay for biological samples.

3.3. Selectivity test for the ALP assay

To test the selectivity of our ALP biosensor, the potential interference of seven biomolecules, namely, penicillin, Try, Thr, BSA, MMP-9, GOX, and IgG, with the ALP biosensor were investigated because these biomolecules are commonly found in human serum [42,46,68]. As shown

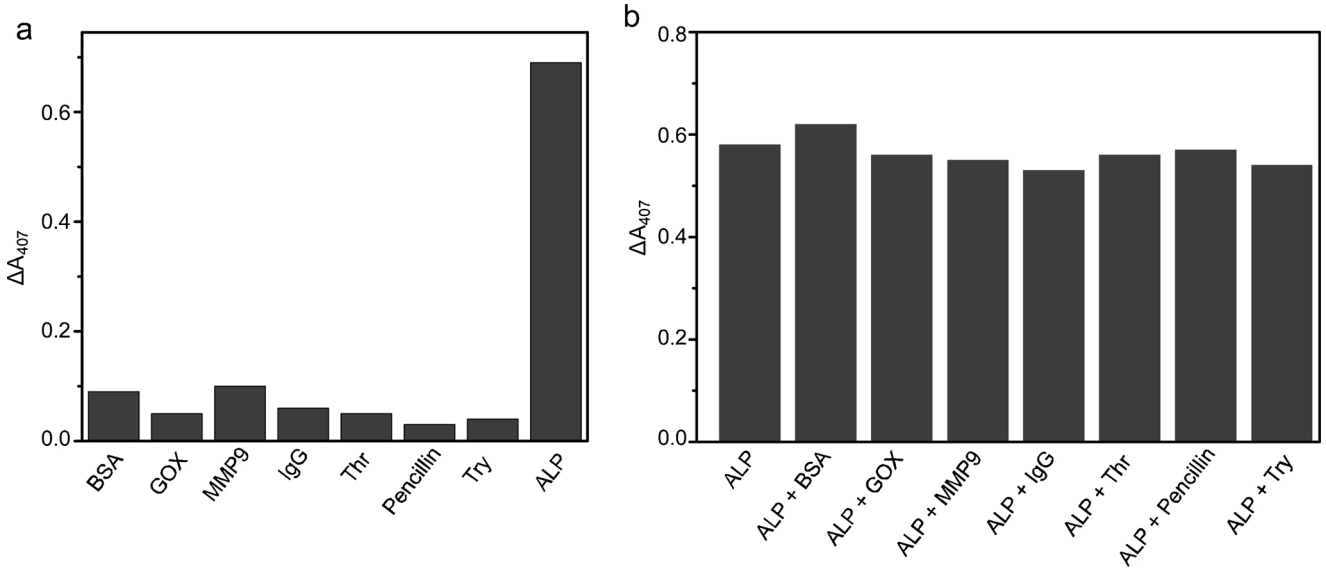

Fig. 3. (**a**) Selectivity test of the ALP biosensor with the seven common biomolecules and ALP. (**b**) Interference test of the ALP biosensor in the presence of the biomolecules and ALP. The concentrations of ALP in the selectivity and interference test were 150 and 100 U/L respectively, whereas the concentrations of BSA, MMP9, penicillin, thrombin, GOX, trypsin, and IgG were 100 μg/mL, 0.2 μg/mL, 500 U/L, 0.5 μg/mL, 50 μg/mL, 100 μg/mL, and 50 μg/mL, respectively.

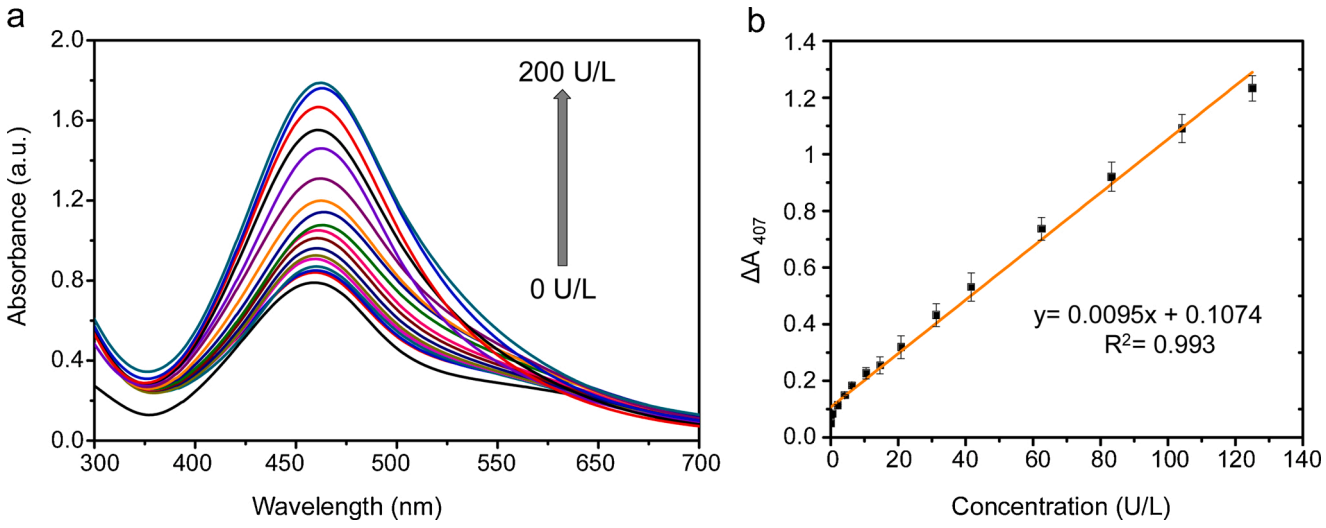

Fig. 4. **(a)** UV–vis spectra of the ALP biosensor with different concentrations of the added ALP in a 10 % diluted human serum solution and **(b)** linear standard addition calibration curve of the change in the absorbance of the biosensor as a function of added ALP concentration.

Table 2
Analytical results of the ALP assay in the 10 % diluted human serum solution using the standard addition method.

Sample	Detected (U/L)	Added (U/L)	Total found (U/L)	Recoveries (%)	RSD (%)
Human serum	11.1	2.1	13.18	99.25	3.25
		6.25	16.99	97.91	4.40
		10.4	21.13	98.27	3.91
		20.8	32.34	101.25	4.75

in Fig. 3a, only ALP caused a sharp change in the absorption intensity at 470 nm compared with a slight change by the other biomolecules (the photograph of color change is shown in Figure S5a). Next, we explored the potential interference of the seven biomolecules with the ALP biosensor in the presence of ALP; no significant interference was observed, as shown in Fig. 3b. The photograph of the ALP biosensor color change is shown in Figure S5b.

3.4. Human serum test of the ALP biosensor

To test the feasibility for prognostic (and diagnostic) analysis, we prepared a 10 % diluted human serum solution and detected the concentration of ALP using the standard addition method. The UV–vis spectra of the ALP biosensor with various concentrations of added ALP are shown in Fig. 4a (the color response of the sensor to the human serum is shown in Figure S6). The change in the absorption intensity at 407 nm (ΔA_{407}) with various concentrations of the added ALP is shown in Fig. 4b. Different concentrations of ALP (2.1, 6.25, 10.4 and 20.8 U/L) were added to the initial concentration of ALP in the 10 % diluted human serum based on the standard addition method, and the initial concentration of ALP is revealed to be 11.1 U/L as clarified in the Table 2. The recovery rates of each solution with the added ALP varied from 97.91%–101.25% with the relative standard deviation (RSD) ranging from 3.25 % to 4.75 %, respectively, proving the potential applicability of our ALP biosensor for clinical tests.

4. Conclusion

We developed a colorimetric ALP biosensor based on the *p*AP-mediated growth of AgNPs for the simple and rapid detection of ALP in human serum. We successfully analyzed a human serum sample comprising unknown ALP concentrations with high precision and high reproducibility using the standard addition method. We used *p*APP as a new substrate for the dephosphorylation of ALP to exploit *p*AP, which does not interfere with the biomolecules in human serum, as a reducing agent for the further growth of AgNPs in the solution containing AgNP seeds and Ag^+ ions. Given the high sensitivity of the LSPR peak intensity to the growth of AgNPs, our ALP biosensor showed a linear dynamic range as wide as 0.5–225 U/L and LOD as low as 0.24 U/L. The developed biosensor exhibited a high recovery rate with a high precision of 99.2 ± 1.5 %, proving its high applicability to clinical prognosis and diagnosis. Thus, we believe that our biosensor can be used as a general analytical tool for the detection of diverse biomolecules based on immunoassay technology using ALP as a labeling agent.

Author contributions

S. M. S. performed most of the experiments, including sample preparation and optical characterizations. B.-S. M., D.-G. P. and D.-H. K conceived and supervised the project. All authors analyzed the data and wrote and revised the manuscript.

Declaration of Competing Interest

The authors declare no competing interests.

Acknowledgment

This work was financially supported by a National Research Foundation of Korea (NRF) grant funded (NRF-2018R1D1A1B07041584, 2021R1C1C2008401, 2020M3H1A1077095).

Appendix A. Supplementary data

Supplementary material related to this article can be found, in the online version, at doi:https://doi.org/10.1016/j.colsurfb.2021.111835.

References

[1] J.L. Millán, Alkaline phosphatases, Purinergic Signal. 2 (2) (2006) 335.
[2] E.E. Kim, H.W. Wyckoff, Reaction mechanism of alkaline phosphatase based on crystal structures: two-metal ion catalysis, J. Mol. Biol. 218 (2) (1991) 449–464.
[3] W. Meyer-Sabellek, P. Sinha, E. Köttgen, Alkaline phosphatase: laboratory and clinical implications, J. Chromatogr. B Biomed. Sci. Appl. 429 (1988) 419–444.
[4] S.A. Rankin, A. Christiansen, W. Lee, D.S. Banavara, A. Lopez-Hernandez, Invited review: the application of alkaline phosphatase assays for the validation of milk product pasteurization, J. Dairy Sci. 93 (12) (2010) 5538–5551.
[5] E.-K. Lim, J.O. Keem, H.-s. Yun, J. Jung, B.H. Chung, Smart nanoprobes for the detection of alkaline phosphatase activity during osteoblast differentiation, Chem. Commun. 51 (15) (2015) 3270–3272.
[6] H.-F. Lu, M.-M. Zhang, D. Wu, J.-L. Huang, L.-L. Zhu, C.-M. Wang, Q.-L. Zhang, Colorimetric and fluorescent dual-mode sensing of alkaline phosphatase activity in L-02 cells and its application in living cell imaging based on in-situ growth of silver nanoparticles on graphene quantum dots, Sens. Actuators B Chem. 258 (2018) 461–469.
[7] E.G. Giannini, R. Testa, V. Savarino, Liver enzyme alteration: a guide for clinicians, Can. Med. Assoc. J. 172 (3) (2005) 367–379.
[8] M.C.-L. Yeung, V.W.-W. Yam, Phosphate derivative-induced supramolecular assembly and NIR-emissive behaviour of alkynylplatinum(ii) terpyridine complexes for real-time monitoring of enzymatic activities, Chem. Sci. 4 (7) (2013) 2928–2935.
[9] C. Huggins, C.V. Hodges, Studies on prostatic cancer. I. The effect of castration, of estrogen and androgen injection on serum phosphatases in metastatic carcinoma of the prostate, CA Cancer J. Clin. 22 (4) (1972) 232–240.
[10] K. Ooi, K. Shiraki, Y. Morishita, T. Nobori, High-molecular intestinal alkaline phosphatase in chronic liver diseases, J. Clin. Lab. Anal. 21 (3) (2007) 133–139.
[11] H.-B. Wang, Y. Li, Y. Chen, Z.-P. Zhang, T. Gan, Y.-M. Liu, Determination of the activity of alkaline phosphatase by using nanoclusters composed of flower-like cobalt oxyhydroxide and copper nanoclusters as fluorescent probes, Microchim. Ichnoanal. Acta 185 (2) (2018) 102–109.
[12] J. Sato, K. Okada, S. Fukuda, R. Sato, J. Yasuda, Y. Naito, Serum activities of tartrate-resistant acid phosphatase and bone specific alkaline phosphatase as indices of bone metabolism in the cow, J. Vet. Med. Sci. 64 (7) (2002) 653–655.
[13] S.S.M. Hassan, H.E.M. Sayour, A.H. Kamel, A simple-potentiometric method for determination of acid and alkaline phosphatase enzymes in biological fluids and dairy products using a nitrophenylphosphate plastic membrane sensor, Anal. Chim. Acta 640 (1) (2009) 75–81.
[14] R. Koncki, D. Ogończyk, S. Głąb, Potentiometric assay for acid and alkaline phosphatase, Anal. Chim. Acta 538 (1) (2005) 257–261.
[15] X.-Y. Yao, Q. Wang, Q. Liu, M. Pang, X.-M. Du, B. Zhao, Y. Li, W.-J. Ruan, Ultrasensitive assay of alkaline phosphatase based on the fluorescent response difference of the metal–Organic framework sensor, ACS Omega 5 (1) (2020) 712–717.
[16] C. Jin, J. He, J. Zou, W. Xuan, T. Fu, R. Wang, W. Tan, Phosphorylated lipid-conjugated oligonucleotide selectively anchors on cell membranes with high alkaline phosphatase expression, Nat. Commun. 10 (1) (2019) 2704.
[17] M.S. Malo, A high level of intestinal alkaline phosphatase is protective against type 2 diabetes mellitus irrespective of obesity, EBioMedicine 2 (12) (2015) 2016–2023.
[18] A.L. Brichacek, C.M. Brown, Alkaline phosphatase: a potential biomarker for stroke and implications for treatment, Metab. Brain Dis. 34 (1) (2019) 3–19.
[19] Y. Shi, M. Yang, L. Liu, Y. Pang, Y. Long, H. Zheng, GTP as a peroxidase-mimic to mediate enzymatic cascade reaction for alkaline phosphatase detection and alkaline phosphatase-linked immunoassay, Sens. Actuators B Chem. 275 (2018) 43–49.
[20] R. Li, Q. Liu, Y. Jin, B. Li, Fluorescent enzyme-linked immunoassay strategy based on enzyme-triggered in-situ synthesis of fluorescent copper nanoclusters, Sens. Actuators B Chem. 281 (2019) 28–33.
[21] W. Xie, M. Tian, X. Luo, Y. Jiang, N. He, X. Liao, Y. Liu, A dual-mode fluorescent and colorimetric immunoassay based on in situ ascorbic acid-induced signal generation from metal-organic frameworks, Sens. Actuators B Chem. 302 (2020) 127180.
[22] Y. He, F. Tian, J. Zhou, Q. Zhao, R. Fu, B. Jiao, Colorimetric aptasensor for ochratoxin A detection based on enzyme-induced gold nanoparticle aggregation, J. Hazard. Mater. 388 (2020) 121758.
[23] G.T. Hermanson, Chapter 22 - enzyme modification and conjugation, in: G. T. Hermanson (Ed.), Bioconjugate Techniques, 3rd ed., Academic Press, Boston, 2013, pp. 951–957.

[24] T.C. Richardson, D.V. Chapman, E. Heyderman, Immunoperoxidase techniques: the deleterious effect of sodium azide on the activity of peroxidase conjugates, J. Clin. Pathol. 36 (4) (1983) 411–414.
[25] K. Ye, L. Wang, H. Song, X. Li, X. Niu, Bifunctional MIL-53(Fe) with pyrophosphate-mediated peroxidase-like activity and oxidation-stimulated fluorescence switching for alkaline phosphatase detection, J. Mater. Chem. B 7 (31) (2019) 4794–4800.
[26] P.F. Li, Y.Y. Liu, W.J. Zhang, N. Zhao, A fluorescent probe for pyrophosphate based on tetraphenylethylene derivative with aggregation-induced emission characteristics, ChemistrySelect 2 (13) (2017) 3788–3793.
[27] F. Wang, C. Zhang, Q. Xue, H. Li, Y. Xian, Label-free upconversion nanoparticles-based fluorescent probes for sequential sensing of Cu2+, pyrophosphate and alkaline phosphatase activity, Biosens. Bioelectron. 95 (2017) 21–26.
[28] H. Liu, M. Li, Y. Xia, X. Ren, A turn-on fluorescent sensor for selective and sensitive detection of alkaline phosphatase activity with gold nanoclusters based on inner filter effect, ACS Appl. Mater. Interfaces 9 (1) (2017) 120–126.
[29] C. Ruan, W. Wang, B. Gu, Detection of alkaline phosphatase using surface-enhanced raman spectroscopy, Anal. Chem. 78 (10) (2006) 3379–3384.
[30] A.M. Ingram, B.D. Moore, D. Graham, Simultaneous detection of alkaline phosphatase and beta-galactosidase activity using SERRS, Bioorg. Med. Chem. Lett. 19 (2009) 1569–1571.
[31] D. Sun, F. Cao, L. Cong, W. Xu, Q. Chen, W. Shi, S. Xu, Cellular heterogeneity identified by single-cell alkaline phosphatase (ALP) via a SERRS-microfluidic droplet platform, Lab Chip 19 (2) (2019) 335–342.
[32] D.B. Craig, J.C.Y. Wong, N.J. Dovichi, Detection of attomolar concentrations of alkaline phosphatase by capillary electrophoresis using laser-induced fluorescence detection, Anal. Chem. 68 (4) (1996) 697–700.
[33] D. Wu, F.E. Regnier, M.C. Linhares, Electrophoretically mediated micro-assay of alkaline phosphatase using electrochemical and spectrophotometric detection in capillary electrophoresis, J. Chromatogr. B, Biomed. Appl. 657 (2) (1994) 357–363.
[34] A.R. Whisnant, S.E. Johnston, S.D. Gilman, Capillary electrophoretic analysis of alkaline phosphatase inhibition by theophylline, Electrophoresis 21 (7) (2000) 1341–1348.
[35] K. Ino, Y. Kanno, T. Arai, K.Y. Inoue, Y. Takahashi, H. Shiku, T. Matsue, Novel electrochemical methodology for activity estimation of alkaline phosphatase based on solubility difference, Anal. Chem. 84 (18) (2012) 7593–7598.
[36] J. Peng, X.X. Han, Q.C. Zhang, H.Q. Yao, Z.N. Gao, Copper sulfide nanoparticle-decorated graphene as a catalytic amplification platform for electrochemical detection of alkaline phosphatase activity, Anal. Chim. Acta 878 (2015) 87–94.
[37] Z. Wu, C.-H. Zhou, L.-J. Pan, T. Zeng, L. Zhu, D.-W. Pang, Z.-L. Zhang, Reliable digital single molecule electrochemistry for ultrasensitive alkaline phosphatase detection, Anal. Chem. 88 (18) (2016) 9166–9172.
[38] R. Breslow, I. Katz, Relative reactivities of p-nitrophenyl phosphate and phosphorothioate toward alkaline phosphatase and in aqueous hydrolysis, J. Am. Chem. Soc. 90 (26) (1968) 7376–7377.
[39] G.N. Bowers Jr., R.B. McComb, A continuous spectrophotometric method for measuring the activity of serum alkaline phosphatase, Clin. Chem. 12 (2) (1966) 70–89.
[40] M.J. Grap, R.S. Burk, V. Lucas, C.L. Munro, P.A. Wetzel, C.M. Schubert, Use of high frequency ultrasound to detect changes in skin integrity: an image evaluation validation procedure, Intensive Crit. Care Nurs. 31 (3) (2015) 141–147.
[41] Y. Liu, M. Pan, W. Wang, Q. Jiang, F. Wang, D.-W. Pang, X. Liu, Plasmonic and photothermal immunoassay via enzyme-triggered crystal growth on gold nanostars, Anal. Chem. 91 (3) (2019) 2086–2092.
[42] Z. Gao, K. Deng, X.-D. Wang, M. Miró, D. Tang, High-resolution colorimetric assay for rapid visual readout of phosphatase activity based on Gold/Silver Core/Shell nanorod, ACS Appl. Mater. Interfaces 6 (20) (2014) 18243–18250.
[43] Y. Li, X. Ma, Z. Xu, M. Liu, Z. Lin, B. Qiu, L. Guo, G. Chen, Multicolor ELISA based on alkaline phosphatase-triggered growth of Au nanorods, Analyst 141 (10) (2016) 2970–2976.
[44] Z. Zhang, Z. Chen, S. Wang, F. Cheng, L. Chen, Iodine-mediated etching of gold nanorods for plasmonic ELISA based on colorimetric detection of alkaline phosphatase, ACS Appl. Mater. Interfaces 7 (50) (2015) 27639–27645.
[45] J. Gao, M. Jia, Y. Xu, J. Zheng, N. Shao, M. Zhao, Prereduction-promoted enhanced growth of silver nanoparticles for ultrasensitive colorimetric detection of alkaline phosphatase and carbohydrate antigen 125, Talanta 189 (2018) 129–136.
[46] M. Luo, X. Xue, H. Rao, H. Wang, X. Liu, X. Zhou, Z. Xue, X. Lu, Simply converting color signal readout into thermal signal readout for breaking the color resolution limitation of colorimetric sensor, Sens. Actuators B Chem. 309 (2020) 127707.
[47] Y. Tang, W. Lai, J. Zhang, D. Tang, Competitive photometric and visual ELISA for aflatoxin B1 based on the inhibition of the oxidation of ABTS, Microchim. Ichnoanal. Acta 184 (7) (2017) 2387–2394.
[48] X. Yan, L. He, C. Zhou, Z.-J. Qian, P. Hong, S. Sun, C. Li, Fluorescent detection of ascorbic acid using glutathione stabilized Au nanoclusters, Chem. Phys. 522 (2019) 211–213.
[49] B.M.M. May, S. Parani, O.S. Oluwafemi, Detection of ascorbic acid using green synthesized AgInS2 quantum dots, Mater. Lett. 236 (2019) 432–435.
[50] K. Dhara, R.M. Debiprosad, Review on nanomaterials-enabled electrochemical sensors for ascorbic acid detection, Anal. Biochem. 586 (2019) 113415.
[51] L. Kong, Y. Gan, T. Liang, L. Zhong, Y. Pan, D. Kirsanov, A. Legin, H. Wan, P. Wang, A novel smartphone-based CD-spectrometer for high sensitive and cost-effective colorimetric detection of ascorbic acid, Anal. Chim. Acta 1093 (2020) 150–159.
[52] S.M. Shaban, J.Y. Lee, D.-H. Kim, Dual-surfactant-Capped Ag Nanoparticles as a highly selective and sensitive colorimetric sensor for citrate detection, ACS Omega 5 (19) (2020) 10696–10703.
[53] S. Bandyopadhyay, G. Singh, W.R. Glomm, Shape tunable synthesis of anisotropic gold nanostructures through binary surfactant mixtures, Mater. Today Chem. 3 (2017) 1–9.
[54] B.N. Khlebtsov, V.A. Khanadeev, J. Ye, G.B. Sukhorukov, N.G. Khlebtsov, Overgrowth of gold nanorods by using a binary surfactant mixture, Langmuir 30 (6) (2014) 1696–1703.
[55] K. Raghunathan, J. Antony, S. Munir, J.-P. Andreassen, S. Bandyopadhyay, Tuning and tracking the growth of gold nanoparticles synthesized using binary surfactant mixtures, Nanoscale Advances 2 (5) (2020) 1980–1992.
[56] S. Padsala, V.I. Patel, D. Ray, V.K. Aswal, P. Bahadur, Mixed micelles of sodium perfluorooctanoate and imidazolium based ionic liquids in aqueous solution: a SANS and Tensiometric study, J. Mol. Liq. 322 (2021) 114558.
[57] R.B. Pereyra, M.D. Fernández Leyes, G.F. Silbestri, G.A. Durand, P.C. Schulz, H. A. Ritacco, E.P. Schulz, Experimental and thermodynamic analysis of mixed micelles formed by dodecylethylmethacrylatedimethylammonium bromide and tetradecyltrimethylammonium bromide, Colloids Surf. A Physicochem. Eng. Asp. 614 (2021) 126118.
[58] D. Shi, Y. Sun, L. Lin, C. Shi, G. Wang, X. Zhang, Naked-eye sensitive detection of alkaline phosphatase (ALP) and pyrophosphate (PPi) based on a horseradish peroxidase catalytic colorimetric system with Cu(ii), Analyst 141 (19) (2016) 5549–5554.
[59] Q. Hu, M. He, Y. Mei, W. Feng, S. Jing, J. Kong, X. Zhang, Sensitive and selective colorimetric assay of alkaline phosphatase activity with Cu(II)-phenanthroline complex, Talanta 163 (2017) 146–152.
[60] Q. Hu, B. Zhou, P. Dang, L. Li, J. Kong, X. Zhang, Facile colorimetric assay of alkaline phosphatase activity using Fe(II)-phenanthroline reporter, Anal. Chim. Acta 950 (2017) 170–177.
[61] N.G. Rojas-Avelizapa, M. Gómez-Ramírez, R. Hernández-Gama, J. Aburto, R. García de León, Isolation and selection of sulfur-oxidizing Bacteria for the treatment of sulfur-containing hazardous wastes, Chem. Biochem. Eng. Q. 27 (1) (2013) 109–117.
[62] C. Tang, Z. Qian, Y. Huang, J. Xu, H. Ao, M. Zhao, J. Zhou, J. Chen, H. Feng, A fluorometric assay for alkaline phosphatase activity based on β-cyclodextrin-modified carbon quantum dots through host-guest recognition, Biosens. Bioelectron. 83 (2016) 274–280.
[63] Z.S. Qian, L.J. Chai, Y.Y. Huang, C. Tang, J. Jia Shen, J.R. Chen, H. Feng, A real-time fluorescent assay for the detection of alkaline phosphatase activity based on carbon quantum dots, Biosens. Bioelectron. 68 (2015) 675–680.
[64] Z. Qian, L. Chai, C. Tang, Y. Huang, J. Chen, H. Feng, Carbon quantum dots-based recyclable real-time fluorescence assay for alkaline phosphatase with adenosine triphosphate as substrate, Anal. Chem. 87 (5) (2015) 2966–2973.
[65] Z. Song, R.T.K. Kwok, E. Zhao, Z. He, Y. Hong, J.W.Y. Lam, B. Liu, B.Z. Tang, A ratiometric fluorescent probe based on ESIPT and AIE processes for alkaline phosphatase activity assay and visualization in living cells, ACS Appl. Mater. Interfaces 6 (19) (2014) 17245–17254.
[66] Y. He, B. Jiao, Determination of the activity of alkaline phosphatase based on the use of ssDNA-templated fluorescent silver nanoclusters and on enzyme-triggered silver reduction, Microchim. Ichnoanal. Acta 184 (10) (2017) 4167–4173.
[67] A.-Z. Xu, L. Zhang, H.-H. Zeng, R.-P. Liang, J.-D. Qiu, Fluorometric determination of the activity of alkaline phosphatase based on the competitive binding of gold nanoparticles and pyrophosphate to CePO4:Tb nanorods, Microchim. Ichnoanal. Acta 185 (6) (2018) 288.
[68] C. Chen, D. Zhao, B. Wang, P. Ni, Y. Jiang, C. Zhang, F. Yang, Y. Lu, J. Sun, Alkaline Phosphatase-Triggered in Situ Formation of Silicon-Containing Nanoparticles for a Fluorometric and Colorimetric Dual-Channel Immunoassay, Anal. Chem. 92 (6) (2020) 4639–4646.